Archives of Biochemistry and Biophysics 536 (2013) 72–80

Contents lists available at SciVerse ScienceDirect

Archives of Biochemistry and Biophysics

journal homepage: www.elsevier.com/locate/yabbi

Biosynthesis of UDP-*N,N′*-diacetylbacillosamine in *Acinetobacter baumannii*: Biochemical characterization and correlation to existing pathways ☆

Michael J. Morrison, Barbara Imperiali *

Department of Chemistry, Massachusetts Institute of Technology, 77 Massachusetts Avenue, Cambridge, MA 02139, United States
Department of Biology, Massachusetts Institute of Technology, 77 Massachusetts Avenue, Cambridge, MA 02139, United States

ARTICLE INFO

Article history:
Received 15 May 2013
Available online 5 June 2013

Keywords:
Bacillosamine
Acinetobacter baumannii
Acetyl transferase
Amino transferase
Bacterial *O*-linked glycosylation
Biosynthesis
UDP-diNAcBac
Glycosylation

ABSTRACT

The Gram-negative, opportunistic pathogen *Acinetobacter baumannii* has recently captured headlines due to its ability to circumvent current antibiotic therapies. Herein we show that the multi-drug resistant (MDR) AYE strain of *A. baumannii* contains a gene locus that encodes three enzymes responsible for the biosynthesis of the highly-modified bacterial nucleotide sugar, UDP-*N,N′*-diacetylbacillosamine (UDP-diNAcBac). Previously, this UDP-sugar has been implicated in the pgl pathway of *Campylobacter jejuni*. Here we report the overexpression, purification, and biochemical characterization of the *A. baumannii* enzymes WeeK, WeeJ, and WeeI that are responsible for the production of UDP-diNAcBac. We also demonstrate the function of the phosphoglycosyltransferase (WeeH), which transfers the diNAcBac moiety to undecaprenyl-phosphate. UDP-diNAcBac biosynthesis in *A. baumannii* is also directly compared to the homologous pathways in the pathogens *C. jejuni* and *Neisseria gonorrhoeae*. This work demonstrates for the first time the ability of *A. baumannii* to generate the highly-modified, UDP-diNAcBac nucleotide sugar found previously in other bacteria adding to the growing list of pathogens that assemble glycoconjugates including bacillosamine. Additionally, characterization of these pathway enzymes highlights the opportunity for investigating the significance of highly-modified sugars in bacterial pathogenesis.

Introduction

An alarming trend in antibiotic resistance continues to escalate among human pathogens. A prime example is *Acinetobacter baumannii*, which has garnered a great deal of attention from the medical community stemming from its capacity to resist a majority of antimicrobial therapies [1]. *A. baumannii* is a Gram-negative, aerobic, non-motile opportunistic pathogen that affects immunocompromised patients in a hospital setting. While much effort has been invested in uncovering the mechanism of action of antibiotic resistance [2,3], little has been accomplished in the understanding of pathogenicity. The AYE strain of *A. baumannii* was originally isolated from the 2001 epidemic outbreak in France resulting in a 26% mortality rate among infected individuals [4,5]. Disturbingly, this strain contains an 86-kb genomic island that encodes for 45 of its 52 resistance genes [6]. This resistance island, the largest identified to date, is responsible for the inactivation of β-lactams, aminoglycosides, chloramphenicol, rifampin, and tetracycline [7].

Extensive work has corroborated the link between virulence and bacterial glycosylation in the model system *Campylobacter jejuni* [8]. An interesting characteristic of virulence in this pathogen is the biosynthesis of the unique, bacterial UDP-diNAcBac sugar and its incorporation into complex glycoconjugates. Importantly, the disruption of the enzymes responsible for its production results not only in the diminished ability of *C. jejuni* to adhere to and invade human epithelial cells, but also a reduction in chick and mouse colonization [9,10]. Three distinct enzymes are employed in the biosynthesis of UDP-diNAcBac. First, a dehydratase catalyzes the NAD^+ dependent C4 oxidation, which promotes elimination of water across the C5–C6 glycosyl bond. This is followed by re-reduction of the α,β-unsaturated system at C6 to generate the UDP-4-keto sugar [11]. Subsequently, an aminotransferase catalyzes the transfer of the amino group from L-glutamic acid to the C4 position of UDP-4-keto in a pyridoxal-dependent manner to generate the UDP-4-amino sugar [11]. Lastly, an acetyl-coenzyme

☆ This work was supported by National Institutes of Health Grant GM097241 (B.I.) and the Biotechnology Training Program T32-GM08334 (M.J.M.).

* Corresponding author at: Department of Biology, Massachusetts Institute of Technology, 77 Massachusetts Avenue, Cambridge, MA 02139, United States. Fax: +1 (617) 452 2419.
E-mail address: imper@mit.edu (B. Imperiali).

0003-9861/$ - see front matter © 2013 Elsevier Inc. All rights reserved.
http://dx.doi.org/10.1016/j.abb.2013.05.011

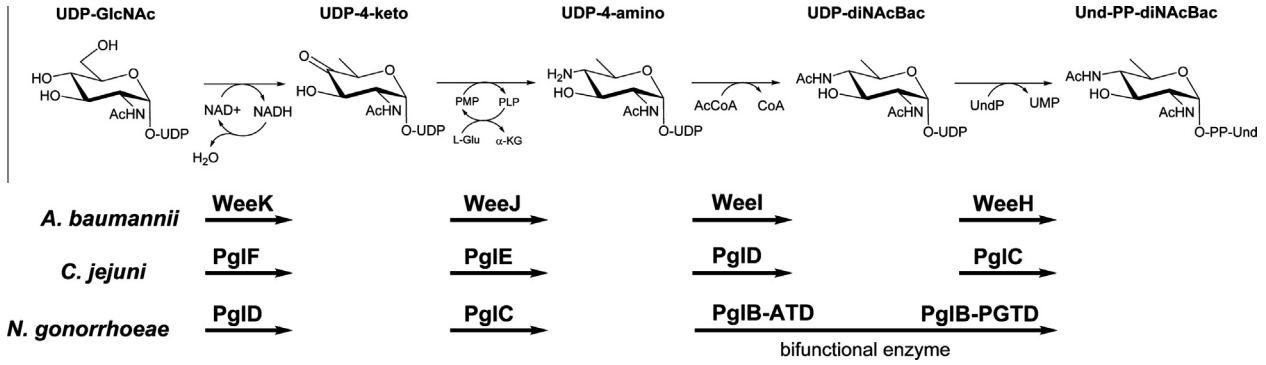

Fig. 1. The UDP-diNAcBac biosynthetic pathway in the AYE strain of *A. baumannii*.

A (AcCoA)[1]-dependent acetyltransferase generates the UDP-diNAcBac sugar nucleotide [12]. Phospho-diNAcBac is then enzymatically transferred to undecaprenyl phosphate and serves as the starting membrane-bound monosaccharide building block for the assembly of more complex oligosaccharides. In *C. jejuni*, the pathway that utilizes UDP-diNAcBac culminates in the transfer of a heptasaccharide onto the side-chain amide nitrogen of asparagine (*N*-linked), whereas the system in *Neisseria gonorrhoeae* transfers a trisaccharide onto a serine or threonine residue (*O*-linked) [13]. Importantly, the first sugar in glycan biosynthesis for this *O*-linked system has been confirmed as UDP-diNAcBac [14].

Bioinformatic analysis of the *C .jejuni* and *N. gonorrhoeae* UDP-diNAcBac systems resulted in the identification of a series of enzymes that catalyze the biosynthesis of UDP-diNAcBac in the AYE strain of *A. baumannii*. The ultimate protein glycosylation steps in these pathways can be classified by the distinct oligosaccharyltransferases; PglB in *C. jejuni* (*N*-linked) and PglO in *N. gonorrhoeae* (*O*-linked). Comparative assessment of their respective oligosaccharyltransferases supported the hypothesis that the AYE strain of *A. baumannii* was an *O*-linked system as it bears a close resemblance to PglO in *N. gonorrhoeae*. Furthermore, genetic analyses based upon sequence homology to their respective *C. jejuni* and *N. gonorrhoeae* enzymes were consistent with a series of analogous proteins (WeeK, WeeJ, and WeeI) responsible for UDP-diNAcBac biosynthesis (Fig. 1). Additionally, a phosphoglycosyltransferase (WeeH) that catalyzes the transfer of phospho-diNAcBac to an undecaprenol phosphate (Und-P) polyisoprenyl carrier was also identified. Given that less virulent strains of *A. baumannii* exist in nature, these genomes were searched for the existence of this biosynthetic pathway to determine its prevalence. While multiple strains contained this particular pathway, the antibiotic susceptible *A. baumannii* strain (ATCC 17978) did not. Instead, this strain contains a distinct *O*-linked glycosylation system with a core GalNAc sugar anchoring a branched pentasaccharide [15]. The terminal *O*-acetylated glucuronic acid sugar (GlcNAc3NAcAOAc) shares homology to a similar pathway in the PAO1 strain of *Pseudomonas aeruginosa* [16] however these enzymes are absent in the AYE strain of *A. baumannii*.

Here we report on the expression, purification, and kinetic characterization of the three enzymes (WeeK, WeeJ, and WeeI) responsible for the biosynthesis of UDP-diNAcBac in the AYE strain of *A. baumannii*. We also determine the substrate specificity of the phosphoglycosyltransferase (WeeH) that catalyzes the transfer of the UDP-activated bacterial sugar onto an Und-P lipid carrier. Furthermore, we discuss the active site homology between *O*- and *N*-linked UDP-diNAcBac pathway proteins in the context of binding and catalysis. This work establishes the presence of the biosynthetic machinery necessary for the production of the UDP-diNAcBac nucleotide sugar in *A. baumannii*. Biochemical characterization of the UDP-diNAcBac biosynthesis pathway in *A. baumannii* is significant in the context of its potential relationship to the more pathogenic and antibiotic resistant strains of this serious human pathogen.

Material and methods

Common materials

All chemicals were purchased from Sigma–Aldrich unless otherwise stated. The UDP-4-keto, UDP-4-amino, and UDP-diNAcBac sugars were biosynthesized as described previously from the *C. jejuni* enzymes PglF, PglE, and PglD [12].

Cloning, expression, and purification

The WeeK, WeeJ, WeeI and WeeH genes were amplified via the polymerase chain reaction (PCR) from the genomic DNA of the AYE strain [4] of *A. baumannii* (ATCC). BamHI and XhoI restriction sites were engineered to facilitate cloning of each construct into the pET-24a(+) vector (Novagen). Amplifications were accomplished with the PfuTurbo DNA Polymerase (Stratagene) as described by the manufacturer. Amplicons were purified and double-digested with BamHI and XhoI restriction enzymes (NE Biolabs). Digested inserts and linearized vectors were fractionated by agarose gel electrophoresis and purified with the Wizard SV Gel and PCR Cleanup Kit (Promega). Ligations were conducted with the T4 DNA ligase kit (Promega) using a 15 min incubation at room temperature. Sequencing by Genewiz (Cambridge, MA) confirmed the presence of all gene products.

The pET24a(+) plasmids containing each gene were used to transform *Escherichia coli* BL21(DE3)pLysS RIL competent cells (Stratagene). One liter of LB media containing 50 μg/mL kanamycin and 30 μg/mL chloramphenicol was inoculated with 8 mL of an

[1] *Abbreviations used: Ab*, *Acinetobacter baumannii*; AcCoA, acetyl-coenzyme A; BSA, bovine serum albumin; CE, capillary electrophoresis; CEF, cell envelope fraction; CHAPS, 3-[(3-cholamidopropyl)dimethylammonio]-1-propanesulfonate; *Cj*, *Campylobacter jejuni*; DDM, *n*-dodecyl-β-D-maltopyranoside; DTNB, 5,5′-dithio-bis-(2-nitrobenzoic acid) or Ellman's reagent; EDTA, ethylenediaminetetraacetic acid; Gal, galactose; GalNAc, *N*-acetylgalactosamine; Glc, glucose; GlcNAc, *N*-acetylglucosamine; IPTG, iso-β-D-thiogalactosylpyranoside; *N*-linked, asparagine-linked; NAD^+, nicotinamide adenine dinucleotide; NDP, nucleotide diphosphate; Ni-NTA, nickel-nitrilotriacetic acid; *O*-linked, serine- or threonine-linked; Pgl, protein glycosylation; PglB-ATD, acetyltransferase domain of PglB; PglB-PGTD, phosphoglycosyltransferase domain of PglB; PSUP, pure solvent upper phase; *Ng*, *Neisseria gonorrhoeae*; TMHMM, tied mixture hidden markov model; UDP, uridine diphosphate; UDP-4-amino, UDP-2-acetamido-4-amino-2,4,6-trideoxy-α-D-glucose; UDP-4-keto, UDP-2-acetamido-4-keto-2,4,6-trideoxy-α-D-glucose; UDP-diNAcBac, UDP-*N*,*N*′-diacetylbacillosamine or UDP-2,4-diacetamido-2,4,6-trideoxy-α-D-glucose; Und-P, undecaprenyl phosphate; Und-PP, undecaprenyl diphosphate.

overnight culture of cells. The cells were then allowed to grow at 37 °C while shaking until they reached an optical density of ~0.8 (λ = 600 nm). The culture was cooled to 16 °C and induced with 0.5 mM iso-β-D-thiogalactosylpyranoside (IPTG). After incubating for 18 h with shaking, the cells were harvested 2600*g* (30 min) and stored at −80 °C until needed.

Each protein purification step was carried out at 4 °C. The cell pellet (~3 g) was resuspended in 40 mL of 50 mM HEPES pH 7.4/100 mM NaCl/30 mM imidazole (Buffer A) and then lysed by sonication. WeeK resuspension buffer was supplemented with 200 μM NAD^+ and WeeJ with 200 μM pyridoxal 5′-phosphate. For WeeJ and WeeI, the lysate was cleared by centrifugation (145,000*g*, 60 min) and added to 2 mL of Ni–NTA resin (Qiagen). The slurry was allowed to tumble for 3 h and then packed into a fritted PolyPrep column (Biorad). The resin was washed with 20 column volumes of Buffer A and then eluted with a buffer containing 50 mM HEPES pH 7.4/100 mM NaCl/ 300 mM imidazole (Buffer B). Fractions containing the purified protein by SDS–PAGE were pooled, dialyzed against 50 mM HEPES pH 7.4/100 mM NaCl (Buffer C) to remove the imidazole, and then supplemented with 15% glycerol. Protein concentrations were calculated based upon the predicted extinction coefficients at λ = 280 nm. Aliquots of the protein were stored at −80 °C until needed.

The membrane-associated proteins WeeK and WeeH required additional purification steps to those of the soluble proteins presented above. Following sonication, cellular debris was cleared at 8000*g* (45 min) and the supernatant was transferred to a clean centrifuge tube. Further centrifugation took place at 145,000*g* (60 min) to pellet the cell envelope fraction (CEF). The CEF was homogenized in 5 mL of Buffer A supplemented with 1% Triton X-100. This solution was allowed to tumble overnight and then subjected to centrifugation 145,000*g* (60 min) to remove any unsolubilized material. The supernatant was combined with 2 mL of Ni–NTA resin and tumbled for 3 h. The slurry was added to a PolyPrep column and washed with 20 column volumes of Buffer A supplemented with 0.1% Triton X-100. The protein was eluted from the resin with Buffer B containing 0.1% Triton X-100. Imidazole was removed through dialysis with Buffer C/0.1% Triton X-100. In the case of WeeH, these dialysis conditions resulted protein precipitation. This issue was remediated by increasing the NaCl concentration in the dialysis buffer to 350 mM. Due to the addition of a UV-active detergent, protein concentrations were calculated with the DC Protein Assay Kit (Biorad). Purified protein was supplemented with 15% glycerol and stored at −80 °C.

Dehydratase (WeeK) activity assay

Kinetic characterization of WeeK utilized capillary electrophoresis (CE) to directly determine UDP-4-keto product formation. The assay contained 50 mM Tris–HCl pH 8.5, 0.005% Triton X-100, 1 mM NAD^+, and varying amounts of UDP-GlcNAc. The reaction was initiated with 0.5 μM WeeK and time points were taken over a time span of 180 min at 25 °C. The reaction was stopped by filtration through a 10 K MWCO membrane (Millipore) to remove the enzyme and the filtrate was injected for 15 s at 30 mbar on a P/ACE MDQ system (Beckman Coulter). Separation of analytes occurred at 20 kV over a 45 min time period on a bare silica capillary (75 μm × 80 cm) with a 25 mM sodium tetraborate (pH 9.3) running buffer and monitored at a λ = 254 nm. Substrate and product peaks were manually integrated utilizing the Beckman 32 Karat software suite. Steady-state rate parameters were calculated from Eq. (1) using the program GraFit 6.0.12 (Erithacus Software). The kinetic parameters are a result of duplicate measurements at each substrate concentration.

$$v = V_{max}[S]/K_m + [S] \quad (1)$$

Aminotransferase (WeeJ) activity assay

Calculation of kinetic constants was carried out as described previously [3]. Briefly, the generation of the UDP-4-amino product from the WeeJ reaction was coupled to an excess of the *C. jejuni* acetyltransferase PglD and the activity of WeeJ was determined by following the production of CoASH at 25 °C. In a flat, clear bottom 96-well plate (Falcon) was added 50 mM HEPES pH 7.4, 0.05% BSA, 0.001% Triton X-100, 1 μM PglD, 400 μM AcCoA, and 400 nM WeeJ. The substrate concentrations of L-glutamate and UDP-4-keto were varied separately to determine kinetic parameters utilizing initial velocity measurements while keeping the other substrate at saturation (10 × K_m). Reactions were initiated with the L-glutamate substrate and quenched with 20% *n*-propanol, 2 mM DTNB (5,5′-dithio-*bis*-(2-nitrobenzoic acid), and 1 mM EDTA over a 30 min time period, which provides a spectroscopic readout for the production of CoA. The absorbance at 415 nm was monitored on an Ultramark EX microplate imaging system (BioRad). Reactions were performed in duplicate and a blank reaction without WeeJ was set up as a background control and subtracted from the final observed reaction rate.

Acetyltransferase (WeeI) activity assay

Kinetic characterization of WeeI was carried out using a previously modified procedure [14]. CoASH generation resulting from the acetyltransferase reaction carried out by WeeI was monitored in the presence of Ellman's reagent (DTNB) through the generation of the TNB^{2-} chromophore in a continuous fashion. To a flat, clear bottom 96-well plate (Falcon) was added 50 mM HEPES pH 7.4, 5 mM $MgCl_2$, 0.05% BSA, 0.001% Triton X-100, 1 mM DTNB, and 1 nM WeeI. Reactions were completed in duplicate and initial rates were measured in the linear portion of the reaction curve over a 5 min time period at 25 °C. The substrate concentrations of AcCoA and UDP-4-amino were varied separately to determine kinetic parameters using initial velocity measurements while holding the other substrate at a saturating level. Due to the solubility and poor binding of UDP-4-amino to WeeI, the AcCoA K_m was determined at K_m of the sugar substrate. A background control in the absence of UDP-4-amino was subtracted from each reaction rate.

Phosphoglycosyltransferase (WeeH) activity assay

A radioactive assay [17] was utilized to establish the UDP-sugar specificity of WeeH. In a 1.5 mL eppendorf tube, 2 nmol of undecaprenyl phosphate was solubilized in 3% DMSO and 1% Triton X-100 by sonication. To this solution was added 30 mM Tris–acetate pH 8.0, 50 mM $MgCl_2$, and 20 μM UDP-sugar (20 mCi/mmol), in a final volume of 100 μL. The reaction was initiated with 200 nM WeeH and time points taken over a 60 min duration at 25 °C. Aliquots of 15 μL were quenched in 1 mL of 2:1 chloroform:methanol mixture and extracted 3 times using 400 μL PSUP (3% chloroform, 49% methanol, 48% water). Following extraction, 5 mL Ecolite(+) scintillation fluid (MP Biomedicals) and 5 mL OptiFluor (Perkin Elmer) were added to the aqueous and organic layers respectively. A Beckman scintillation counter (LS6500) was employed to determine the radioactivity in each sample.

Results

Expression and purification of WeeK, WeeJ, WeeI, and WeeH

Full-length WeeK, WeeJ, WeeI, and WeeH were cloned from the AYE genomic DNA and ligated into the pET-24a(+) vector. Each protein contained an N-terminal T7 tag and a C-terminal His_6 tag

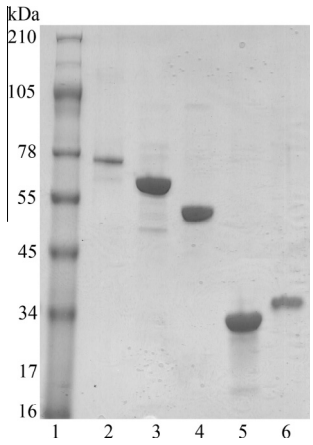

Fig. 2. SDS–PAGE gradient gel (4–20%) of a MW standard (lane 1), WeeK (lane 2), $WeeK_{140}$ (lane 3), WeeJ (lane 4), WeeI (lane 5), and WeeH (lane 6).

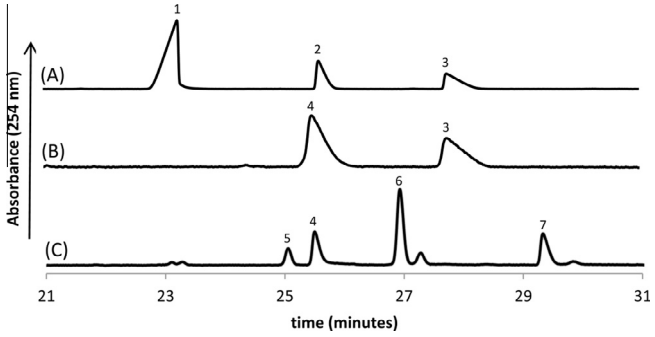

Fig. 3. Electropherogram trace representing the WeeK (A), WeeJ (B), and WeeI reactions (C). Each numbered peak corresponds to a specific analyte: (1) NAD^+; (2) UDP-GlcNAc; (3) UDP-4-keto; (4) UDP-4-amino; (5) UDP-diNAcBac; (6) AcCoA; (7) CoA.

for purification purposes. Following overexpression in *E. coli* BL21 RIL cells and purification with Ni–NTA resin, multi-mg quantities were achieved for each protein from 1 L of culture: WeeK (3 mg), WeeJ (62 mg), WeeI (81 mg), WeeH (2.9 mg). WeeJ was preincubated with excess PLP throughout the entire purification procedure. The stoichiometry of bound PLP to WeeJ ratio was established as 0.9:1 based upon the extinction coefficient of the cofactor ($6600\ M^{-1}\ cm^{-1}$) at an absorbance of 390 nm in 0.1 M NaOH. Membrane proteins WeeK and WeeH were solubilized from the lipid membrane with Triton X-100 detergent. Purity for each protein was assessed by SDS–PAGE to be >95% (Fig. 2). Full-length constructs were confirmed through Western blot analysis probing with antibody for the T7 and His_6 tags. Storage of proteins for >6 months at −80 °C had no affect on enzyme activity.

Functional and kinetic characterization of the dehydratase WeeK

Activity of the full-length WeeK was first investigated with the previously characterized *C. jejuni* dehydratase substrates NAD^+ and UDP-GlcNAc. Substrate turnover was followed by capillary electrophoresis utilizing the UV absorbance of uridine at 254 nm (Fig. 3A). After an overnight reaction at 1 μM of WeeK, <5% of the UDP-4-keto product was observed. A control reaction containing the UDP-4-keto sugar product in the same reaction buffer was run in parallel to ensure that this component was stable for the duration of the assay. Steps were taken to understand the very poor of activity for this enzyme. The presence of divalent metals ($MgCl_2$, $MnCl_2$, $ZnCl_2$, and $CaCl_2$) yielded no improvement in product formation (data not shown). Furthermore, varying amounts of salt (NaCl and KCl) produced a similar result. WeeK was also unable to catalyze the reaction containing the substrate pairs UDP-GalNAc/NAD^+ or UDP-GlcNAc/$NADP^+$. Two additional detergents were utilized for purification in the anticipation of stabilizing a soluble, active protein. In both cases, *n*-dodecyl-β-D-maltopyranoside (DDM) and 3-[(3-cholamidopropyl)dimethylammonio]-1-propanesulfonate (CHAPS) resulted in less substrate turnover than the aforementioned Triton X-100 purified material. Lastly, buffer and pH were examined for their effect on dehydratase activity in an in vitro activity assay. While alternate buffer solutions yielded no improvement in activity, pH had a substantial effect. Increasing the pH from 7.4 to 8.5 resulted in a 10-fold increase of the UDP-4-keto product formation. All further experiments utilized the Triton X-100 detergent purified protein at a buffer pH of 8.5.

WeeK is annotated in the NCBI protein database as a UDP-glucose 4-epimerase, which would reversibly convert UDP-glucose into UDP-galactose. To test this, WeeK was incubated with 1 mM of either UDP-glucose or UDP-galactose for 18 h at room temperature in the presence of 1 mM NAD^+. Following analysis of these reactions by CE, it was concluded that WeeK does not convert UDP-glucose/UDP-galactose to their respective C4 epimers (data not shown). Based upon experimental evidence, we conclude that WeeK is not an epimerase and instead exhibits only NAD^+ dependent dehydratase activity.

With a reliable and robust WeeK CE assay in place, steps were taken to measure the kinetic rate constants of UDP-GlcNAc. The UDP-GlcNAc was varied over a substrate concentration of 0.8–200 μM at 1 mM NAD^+. UDP-4-keto formation was quantified by integrating the area under the product peak from the CE electropherogram trace. The reaction velocities generated from product formation were an average from two separate experiments. These data were plotted versus substrate concentration with Eq. (1) (Fig. S1A) to yield the kinetic parameters in Table 1. For comparison, the previously calculated *C. jejuni* NAD^+-dependent dehydratase (PglF) values are included in the table. Inhibition of WeeK activity was observed at high concentrations of substrate (>500 μM) and therefore not included in the final analysis.

Based upon previous studies with the *C. jejuni* PglF [11,12], the transmembrane domain was removed through cloning to yield the soluble domain of WeeK. This soluble construct improves upon the low yield from full-length construct purification and allows for a facile way to biosynthesize large amounts of UDP-4-keto. To define the appropriate truncation, a sequence alignment with $PglF_{130}$ and examination of a hydropathy plot with TMHMM [18] resulted in the removal of 140 amino acids from the N-terminus ($WeeK_{140}$). Expression and purification in the pET-24a(+) vector resulted in a 28 mg/L of culture yield at >95% purity by SDS–PAGE This

Table 1
Steady-state kinetic parameters for *A. baumannii* and *C. jejuni* dehydratase enzymes.

Dehydratase	Substrate	K_m (μM)	k_{cat} (s^{-1})	k_{cat}/K_m ($M^{-1}\ s^{-1}$)
WeeK	UDP-GlcNAc	5.8 ± 1.2	$2.7 \times 10^{-3} \pm 1.2 \times 10^{-4}$	466
$WeeK_{140}$	UDP-GlcNAc	23 ± 4.5	$4.7 \times 10^{-4} \pm 1.7 \times 10^{-5}$	20
PglF[a]	UDP-GlcNAc	7000	0.12	17

[a] Kinetic parameters published in Ref. [2].

Table 2
Steady-state kinetic parameters for *A. baumannii*, *C. jejuni*, and *N. gonorrhoeae* aminotransferase enzymes.

Aminotransferase	Substrate	K_m (μM)	k_{cat} (s^{-1})	k_{cat}/K_m ($M^{-1}\ s^{-1}$)
WeeJ	UDP-4-keto	1003 ± 110	0.030 ± 0.002	30
WeeJ	L-glutamate	25,000 ± 1900	0.17 ± 0.004	6.7
PglE	UDP-4-keto	366 ± 57	2.4 ± 0.1	6600
PglE	L-glutamate	11,000 ± 340	0.028 ± 0.0003	2.6
PglC[a]	UDP-4-keto	233 ± 35	0.038 ± 0.001	164
PglC[a]	L-glutamate	4900 ± 900	0.025 ± 0.01	5.1

[a] Kinetic parameters published in Ref. [14].

construct catalyzed the conversion of UDP-GlcNAc to UDP-4-keto, however at a reduced rate with respect to the full-length protein. Kinetic characterization of UDP-GlcNAc for $WeeK_{140}$ was carried out (Fig. S1B) and compared directly to the full-length construct in Table 1.

Functional and kinetic characterization of the aminotransferase WeeJ

Capillary electrophoresis was initially utilized to confirm the conversion of UDP-4-keto to UDP-4-amino by WeeJ (Fig. 3B). Since this readout allows for direct comparison of substrates and products, standards of each UDP-sugar were run in parallel with this reaction. UDP-4-keto sugar biosynthesized from the *C. jejuni* and *N. gonorrhoeae* pathways resulted in the production of UDP-4-amino by WeeJ in both cases. These results confirm that the *A. baumannii* enzyme exhibits aminotransferase activity with same stereospecificity observed previously from the *C. jejuni* (PglE) and *N. gonorrhoeae* (PglC) aminotransferases and confirms our analysis that WeeK does not show epimerase activity. To determine the kinetic constants for the substrates L-glutamate and UDP-4-keto, an in vitro assay coupling the production of UDP-4-amino to the *C. jejuni* acetyltransferase PglD was developed. In the presence of Ellman's reagent, generation of the TNB^{2-} chromophore ($\varepsilon_{412\ nm}$ = 14,150 $M^{-1}\ cm^{-1}$) indicates that acetylation of the UDP-4-amino sugar has transpired. Kinetic characterization of each substrate occurred at saturating levels (10 × K_m) of the other substrate to ensure the rate of reaction was dependent only upon the concentration of varying substrate. Typical Michaelis–Menten kinetics were observed for all concentrations of L-glutamate (1.6–200 mM) and UDP-4-keto sugar (0.03–4 mM) (Fig. S2). Initial velocity measurements were averaged between two separate runs and plotted to yield the final kinetic parameters in Table 2.

Functional and kinetic characterization of the acetyltransferase WeeI

Similar to the characterization of WeeJ, a capillary electrophoresis assay confirmed that WeeI produced UDP-diNAcBac from the UDP-4-amino substrate generated by the *C. jejuni* and *N. gonorrhoeae* pathways (Fig. 3C). A continuous, in vitro assay relying on the generation of the TNB^{2-} chromophore from Ellman's reagent was again employed. Initial attempts to determine kinetic parameters for UDP-4-amino resulted in an atypical sigmoidal binding curve suggestive of positive cooperativity (Hill coefficient = 2)

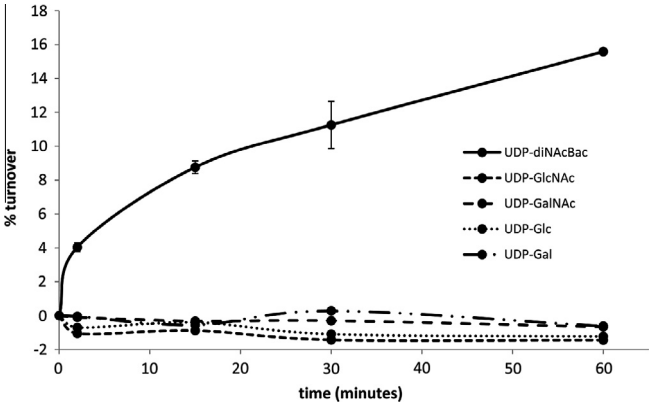

Fig. 4. Specificity of the *A. baumannii* phosphoglycosyltransferase WeeH in the presence of an assortment of UDP-sugars. Aliquots of the reaction containing 2 nmol Und-P, 1% Triton X-100, 3% DMSO, 30 mM TRIS–acetate pH 8.0, 50 mM MgCl2, 40 μM UDP-sugar, 20 μM UDP-GalNAc (20 mCi/mmol), 4.5 μM *C. jejuni* PglA, and 200 nM WeeH were taken over a 30 min time course. Error bars represent standard deviation from triplicate measurements.

(data not shown). Further experiments were applied to establish that WeeI activity was dependent upon $MgCl_2$. In the presence of EDTA, WeeI retained the ability for substrate turnover establishing that $MgCl_2$ is not essential for catalytic function of this enzyme. Comparison of the reaction rates indicated a 6.4-fold increase in activity with the addition of 5 mM divalent magnesium. The presence of $MgCl_2$ resulted in typical Michaelis–Menten kinetics over a range of AcCoA (0.02–2 mM) and UDP-4-amino (0.08–10 mM) concentrations (Fig. S3). As a result of the poor binding of UDP-4-amino to WeeI, the apparent AcCoA K_m was determined at a UDP-4-amino concentration of 4 mM (at K_m). Kinetic parameters listed in Table 3 are the outcome of initial velocity measurements repeated in duplicate.

Substrate specificity of the phosphoglycosyltransferase WeeH

Substrate specificity of WeeH was determined using a previously established radioactivity-based assay [14,19]. This method relied on the transfer of a tritium-labeled phospho-sugar (from the UDP-activated substrate) to a hydrophobic undecaprenyl phosphate. The polyprenyldiphosphate-monosaccharide product (Und-PP-diNAcBac) is extracted into the organic phase separating it from the aqueous soluble unreacted radioactive UDP-diNAcBac. In total, five UDP-sugars were analyzed for their ability to act as a substrate for WeeH. This phosphoglycosyltransferase exhibited clear selectivity for UDP-diNAcBac over all other UDP-sugars (UDP-GlcNAc, UDP-GalNAc, UDP-Glc, UDP-Gal) (Fig. 4).

Active site comparison between O- and N-linked UDP-diNAcBac pathway proteins

To better understand the relationship between UDP-diNAcBac pathways in the *O*- and *N*-linked systems, active site sequence homology was investigated with an emphasis on the

Table 3
Steady-state kinetic parameters for *A. baumannii*, *C. jejuni*, and *N. gonorrhoeae* acetyltransferase enzymes.

Acetyltransferase	Substrate	K_m (μM)	k_{cat} (s^{-1})	k_{cat}/K_m ($M^{-1}\ s^{-1}$)
WeeI	UDP-4-amino	4300 ± 140	$1.1 \times 10^4 \pm 1.7 \times 10^2$	2.6×10^6
WeeI	AcCoA	110 ± 6.0	$3.5 \times 10^3 \pm 5.5 \times 10^1$	3.2×10^7
PglD	UDP-4-amino	311 ± 23	$1.2 \times 10^4 \pm 3.8 \times 10^2$	4.0×10^7
PglD	AcCoA	194 ± 30	$1.1 \times 10^4 \pm 5.0 \times 10^2$	5.5×10^7
PglB-ATD	UDP-4-amino	192 ± 26	$2.0 \times 10^3 \pm 8.2 \times 10^1$	1.0×10^7
PglB-ATD	AcCoA	338 ± 47	$2.3 \times 10^3 \pm 1.1 \times 10^2$	6.9×10^6

aminotransferase and acetyltransferase enzymes in the *C. jejuni*, *N. gonorrhoeae*, and *A. baumannii* pathways. The NAD^+-dependent dehydratase enzymes were excluded from this comparative analysis since structures of these enzymes have not yet been determined.

To define the binding pocket for the aminotransferase PglE from the *N*-linked glycosylation pathway, the structural analysis of a homologous enzyme from *Helicobacter pylori* (PseC) was employed [20]. A crystal structure of PseC with the bound external aldimine (2FNU) was aligned with the PLP bound PglE (1O61) crystal structure to define the active site residues [21]. PseC catalyzes the transamination reaction at the C4 position of a UDP-activated sugar similar to the PglE UDP-4-keto substrate. In this case, the only variation is the stereochemistry of the methyl group at the C5 position (β-L-arabino-hexulose as opposed to α-D-xylo-hexulose). Alignment of the PseC and PglE structures resulted in a root mean square (rms) value of 1.1 Å for the monomer and a rms value of 0.6 Å for the active site residues. A second aminotransferase structure from *P. aeruginosa* (WbpE) containing the bound external aldimine was used to provide further support for the PseC findings [22]. The residues defining the PglE active site were identical in both examples. The aminotransferase binding pocket was defined to a 5 Å distance from the external aldimine-bound molecule in the structural visualization program PyMOL (Fig. 5) [23]. Sequence alignment of the *N. gonorrhoeae* (PglC) and *A. baumannii* (WeeJ) aminotransferases to PglE was accomplished using Clustal Omega. The final alignment among the three aminotransferases was visually represented by the program Jalview (Fig. S4) [24]. While the overall sequence identity between *O*-linked and *N*-linked aminotransferases is relatively low, the enzymes from the *O*-linked glycosylation pathway (PglC and WeeJ) exhibit exceptionally high homology (67% sequence identity) (Table 4). This observation is even more apparent when comparing the residues within the active site. Not surprisingly, the catalytic lysine residue responsible for product formation is completely conserved among the *C. jejuni* (K184), *N. gonorrhoeae* (K185), and *A. baumannii* (K185) aminotransferases (Fig. 6). Six of the ten PseC-binding residues interact with PLP and homologous amino acids can be accounted for in the PglE structure. Of note, the PglE residues D155, S179, N227 and T57 are completely conserved among the three

Table 4
Sequence identity for *A. baumannii* (*Ab*), *C. jejuni* (*Cj*), and *N. gonorrhoeae* (*Ng*) aminotransferase enzymes.

Aminotransferase pair	Total protein (%)	External aldimine active site (%)
PglE(*Cj*)/PglC(*Ng*)	22	38
PglE(*Cj*)/WeeJ(*Ab*)	18	38
WeeJ(*Ab*)/PglC(*Ng*)	67	90

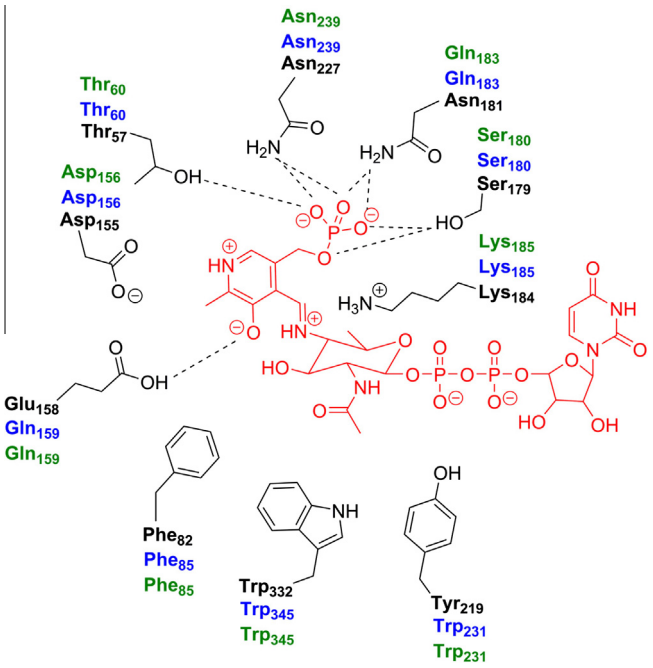

Fig. 6. Illustration of the relevant amino acids responsible for the aminotransferase binding pocket in PglE(*Cj*). Residues labeled in blue and green represent analogous positions in PglC(*Ng*) and WeeJ(*Ab*) respectively. (For interpretation of the references to color in this figure legend, the reader is referred to the web version of this article.)

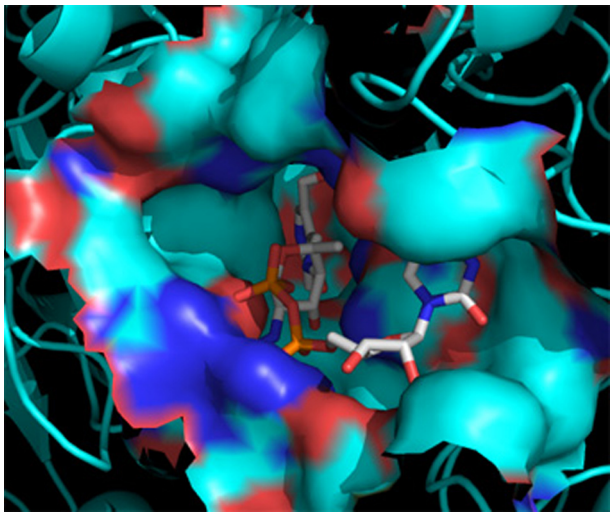

Fig. 5. Surface representation of *C. jejuni* PglE binding pocket. The crystal structure of the homologous aminotransferase PseC bound to the PMP-UDP-L-AltNAc external aldimine (2FNU) was utilized to define the active site. Following alignment with the PLP-bound PglE crystal structure (1O61), amino acids within 5 Å of the external aldimine were identified as binding-pocket residues.

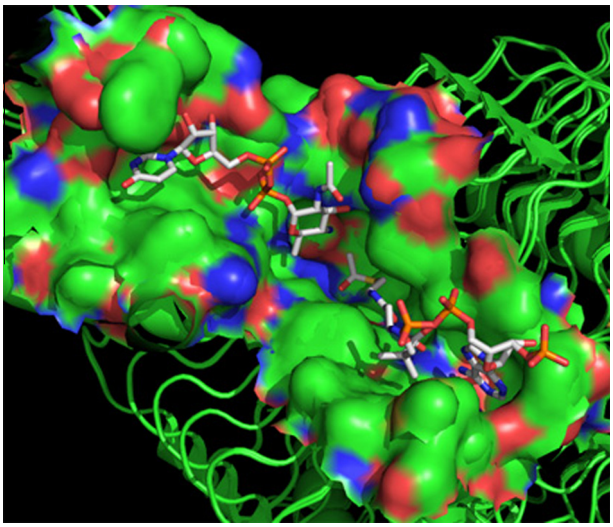

Fig. 7. Surface representation of the *C. jejuni* PglD binding pocket. Amino acid residues within 5 Å of the UDP-4-amino (top left) and AcCoA (bottom right) substrates were classified as contributing to the acetyltransferase active site. Binding pocket identification relied on the UDP-4-amino (3BSS) and AcCoA (3BSY) bound PglD crystal structures.

Table 5
Sequence identity for *A. baumannii* (*Ab*), *C. jejuni* (*Cj*), and *N. gonorrhoeae* (*Ng*) acetyltransferase enzymes.

Acetyltransferase pair	Total protein (%)	AcCoA active site (%)	UDP-4-amino active site (%)
PglD(*Cj*)/PglB-ATD(*Ng*)	34	37	64
PglD(*Cj*)/WeeI(*Ab*)	26	34	48
WeeI(*Ab*)/PglB-ATD(*Ng*)	26	56	42

aminotransferases and associate directly with PLP. While E158 and N181 are not identical in the *N. gonorrhoeae* and *A. baumannii* model, a similar role can be hypothesized by glutamine at both positions. Only Y316 in the PseC structure has direct interaction with the sugar moiety. No obvious counterpart can be identified in the sequence alignment with PglE, PglC, and WeeJ.

In order to establish the acetyltransferase binding pockets of WeeI and PglB-ATD, the *C. jejuni* PglD crystal structures containing bound UDP-4-amino (3BSS) and AcCoA (3BSY) were utilized [25]. Each binding site was defined as for the aminotransferases, with a 5 Å distance surrounding the respective substrate (Fig. 7). Sequence alignment and visualization were again accomplished utilizing Clustal Omega and Jalview (Fig. S5). Interestingly, the sequence identity of both active sites varies highly depending upon the specific substrate-binding pocket and acetyltransferase pair being examined (Table 5). The AcCoA binding site exhibits more homology between the *O*-linked (WeeI/PglB-ATD) pathway enzymes. The majority of interactions between AcCoA and protein side chains occur at the carbonyl oxygen of the thioester (Fig. 8A). The nucleotide and pantetheine moieties of AcCoA are held in the substrate-binding site by a network of water molecules and backbone interactions from I155 to G173, which are represented by threonine and glycine in the *O*-linked acetyltransferase enzyme sequences. Unexpectedly, the UDP-4-amino binding pocket shares more similarity between *N*-linked PglD and *O*-linked PglB-ATD. Interactions between the pyranose C4 amine (H125), the ribosyl 3′ hydroxyl group (D35), and the uridine imide (D36) are exclusively conserved (Fig. 8B). The uracil of the NDP sugar is stabilized by a similar hydrophobic pocket (Y10, I55, I60, and

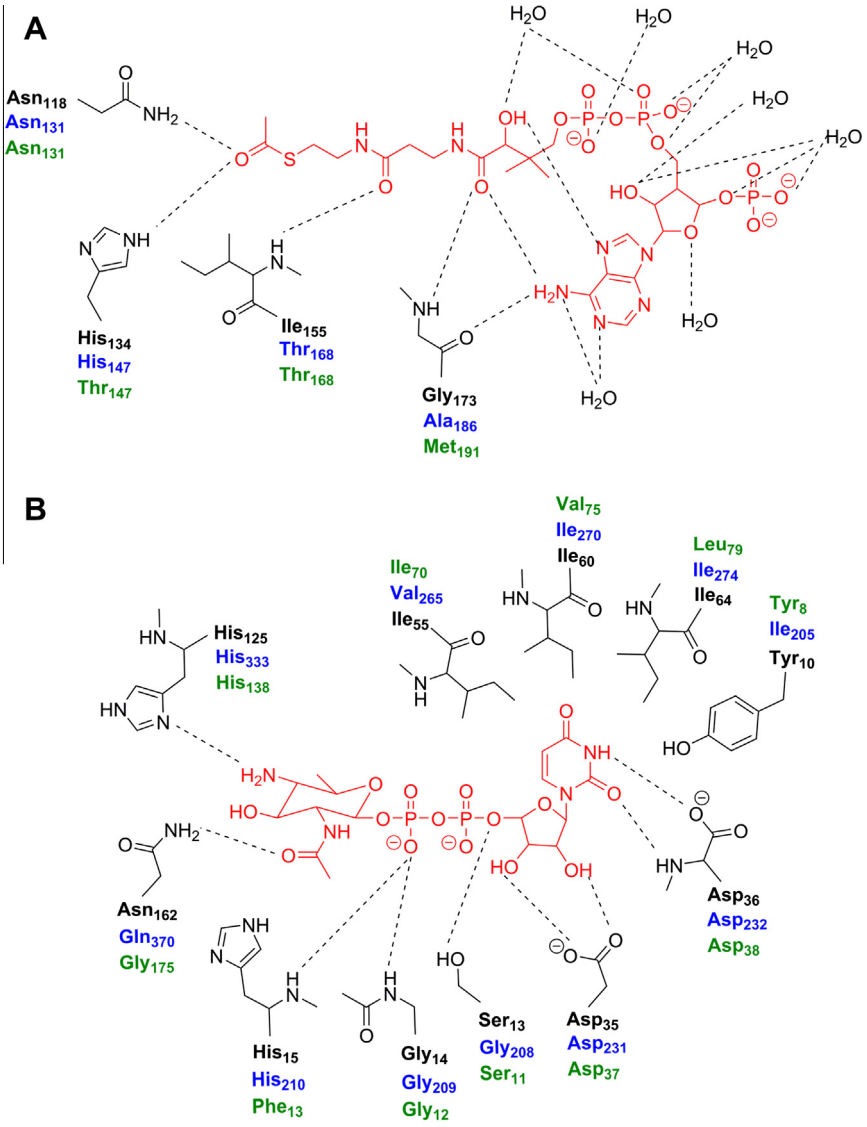

Fig. 8. Illustration of the relevant amino acids responsible for the AcCoA (A) and UDP-4-amino (B) binding pockets in PglD(*Cj*). Residues labeled in blue and green represent analogous positions in PglB(*Ng*)ATD and WeeI(*Ab*) respectively. (For interpretation of the references to colour in this figure legend, the reader is referred to the web version of this article.)

I64) in PglB-ATD and WeeI model structures. There are two major differences in the proposed WeeI UDP-4-amino binding pocket with respect to PglD. The asparagine at position 162 that interacts with the carbonyl oxygen of the pyranose C2 acetyl group is replaced with a glycine (G175). Importantly, the H15 residue that interacts with the sugar substrate β-phosphate moiety and inserts into the pocket to accommodate UDP-4-amino is replaced with a phenylalanine (F13).

Discussion

The A. baumannii enzymes WeeK, J, and I produce UDP-diNAcBac

Previous studies have focused on characterizing the UDP-diNAcBac glycosylation pathway enzymes in *N*-linked (*C. jejuni*) [12] and *O*-linked (*N. gonorrhoeae*) [14] systems. The finding that the AYE strain of *A. baumannii* contains an *O*-linked bacillosamine biosynthesis pathway further confirms the connection between the sugar and glycoconjugates that may be involved in pathogenicity while adding to the growing number of bacteria with this system. This strain of *A. baumannii* is of particular interest due to its extreme antibiotic resistance. Understanding the virulence factors associated with *A. baumannii* is of great importance to the medical community particularly as a potential new target in efforts to address the ever-growing resistance to current antibiotics. The *A. baumannii* dehydratase (WeeK), aminotransferase (WeeJ), and acetyltransferase (WeeI) were individually investigated for their ability to catalyze their anticipated substrates and characterized kinetically. Activity assays with UDP-sugar substrates generated from the *C. jejuni* and *N. gonorrhoeae* glycosylation pathways confirmed that the *A. baumannii* enzymes utilize the same general mechanism to produce UDP-diNAcBac. From a kinetic viewpoint, it appears that this pathway uses a similar overall strategy employed by homologous enzymes in *C. jejuni* and *N. gonorrhoeae*. Specifically, the committed step in UDP-diNAcBac biosynthesis is controlled by the first and rate-limiting enzyme on this pathway (WeeK) while the final acetylation of UDP-4-amino by WeeI provides the most catalytically efficient reaction. Collectively, these enzymes are responsible for the biosynthesis of the highly-modified bacterial NDP sugar, UDP-diNAcBac. While the main focus of this paper has been on the characterization of the early pathway enzymes responsible for UDP-diNAcBac biosynthesis, composition of the final protein-linked oligosaccharide is still unknown.

UDP-diNAcBac enzyme diversity in N- and O-linked glycosylation

Previous kinetic characterization of the *C. jejuni* dehydratase PglF resulted in a K_m of 7 mM and a k_{cat} of 0.12 s^{-1} [12]. Surprisingly, the *A. baumannii* WeeK binds to UDP-GlcNAc with a significantly higher affinity (1000-fold) however catalyzes this reaction at an appreciably reduced rate (44-fold). As a result, WeeK is a catalytically more efficient enzyme (k_{cat}/K_m = 466 M^{-1} s^{-1}) relative to PglF (k_{cat}/K_m = 17 M^{-1} s^{-1}). The two NAD^+-dependent dehydratases have a sequence identity (31%) that is similar to other homologous proteins on this pathway yet exhibit contrasting kinetic parameters. It is interesting that WeeK binds UDP-GlcNAc with such high affinity since this substrate is utilized for many other pathways within the cell including biofilm formation [26], lipooligosaccharide [27], and various cell envelope components.

To define the WeeJ aminotransferase UDP-sugar binding pocket, a homologous structure from *H. pylori* (PseC) was employed (Fig. 5). When comparing the sequence identities of the three aminotransferases (overall and active site), a trend emerges (Table 4). While the *N*-linked *C. jejuni* aminotransferase catalyzes the same reaction, it shares little in identity to its *O*-linked relatives. This observation however is not reflected in the catalytic efficiency for the substrate L-glutamate (Table 2) as all three aminotransferases share comparable kinetic parameters. When evaluating catalytic efficiency for the UDP-4-keto substrate in relation to its sequence, a different story unfolds. PglE has an elevated rate of turnover in comparison to the *O*-linked pathway proteins that result in a 39-fold (PglC) and 217-fold (WeeJ) increase in catalytic efficiency. In contrast, PglC and WeeJ share a similar albeit lower efficiency for UDP-4-keto catalysis.

The final step in the biosynthesis of UDP-diNAcBac is catalyzed by the acetyltransferase WeeI. The AcCoA and UDP-4-amino binding pockets have been well established through *C. jejuni* PglD crystallographic analysis (Fig. 7) [25]. While a clear trend was established when comparing *O*-linked versus *N*-linked aminotransferases, a different picture emerges with the acetyltransferase enzymes. With respect to sequence identities, PglD and PglB-ATD from *N. gonorrhoeae* share greater homology in all aspects apart from the AcCoA binding pocket (Table 5). This is a surprising observation when relating these results with homology between both the dehydratases and aminotransferases. It is apparent that the gene products of UDP-diNAcBac biosynthesis in *A. baumannii* were acquired collectively as they are located consecutively in the same operon. It is not currently understood why changes to the acetyltransferase binding pocket may have occurred with respect to the substrate affinity and fitness of this particular strain of the bacterium. The similarity in AcCoA kinetic parameters (Table 3) is directly reflected in the conserved residues for cofactor binding. Unexpectedly, PglD and PglB-ATD share a higher homology in their UDP-4-amino binding sites relative to WeeI (Table 5). Many of the residues that interact with the UDP-sugar are strictly conserved across all three acetyltransferases. Surprisingly, WeeI exhibits poor affinity for UDP-4-amino with respect to the other acetyltransferases (>10-fold). Only two major differences are observed in the sugar-binding pocket (Fig. 8B). First, an asparagine side chain that interacts with the carbonyl oxygen of the pyranose C2 acetyl group in the PglD structure is replaced with glycine. However, an adjacent glutamine in WeeI may serve as a hydrogen-bond donor depending upon its location within the tertiary structure. Second and seemingly more noteworthy is the replacement of histidine (H15) with phenylalanine in WeeI (F13). This residue interacts with the sugar substrate β-phosphate and repositions in the pocket to accommodate UDP-4-amino. Therefore, this amino acid is positioned to act as a gatekeeper for sugar substrate binding. The hydrophobicity and size of this residue with respect to histidine may partially explain the poor affinity of this substrate towards WeeI (Table 3).

Enzymatic flux through the UDP-diNAcBac pathway

To eliminate adverse byproducts and off-pathway reactions, nature often exploits substrate channeling, wherein intermediates are shuttled to successive enzymes to increase the efficiency of a particular pathway. In the case of the UDP-diNAcBac biosynthesis, the initial NAD^+-dependent dehydratase is catalytically inefficient with respect to the subsequent enzymes in the pathway [12,28]. Nevertheless, interpretation of these assay results must be viewed with some caution since the in vitro analysis conditions may not reflect the true kinetic potential of the membrane-bound dehydratase in its natural cellular environment. WeeK appears to function as a gatekeeper to UDP-diNAcBac production as the formation of the UDP-4-keto sugar is the rate-limiting step. In order to drive this pathway forward, downstream enzymes appear to be tuned to increase their catalytic efficiency. In all three acetyltransferases examined in this paper, the catalysis of UDP-4-amino to UDP-diNAcBac is significantly elevated with respect to the earlier pathway enzymes. The high catalytic efficiency of the acetyltransferase

drives the production of UDP-diNAcBac by rapidly consuming UDP-4-amino and in turn promotes the conversion of more UDP-GlcNAc to UDP-4-keto. A similar effect can be observed in the biosynthesis of UDP-ManNAc(3NAc)A in *P. aeruginosa*; [16] additionally, this type of flux is prevalent in metabolic pathways. For example, glycolytic flux in bacteria utilizes a feed-forward loop where high levels of fructose-1,6-bisphosphate signal for increased activity of glyceraldehyde 3-phosphate dehydrogenase (GAPDH) [29,30]. Pyruvate kinase (PK) is also part of this loop and its activity is responsible for flux into the lower half of glycolysis. Metabolic flux control is also elicited through the pyruvate node during anaerobic growth in *E. coli* to maintain redox balance in the cell [31]. UDP-diNAcBac biosynthesis is yet another example of flux created by a highly active enzyme at the terminal end of the pathway that can overcome the deficient catalytic efficiency of preceding enzymes.

These studies establish details of the characterization of the early UDP-diNAcBac pathway proteins WeeK, WeeJ, WeeI, and WeeH. Comparison to the analogous *C. jejuni* and *N. gonorrhoeae* systems has resulted in an understanding of the similarities and differences between *N*- and *O*-linked glycosylation pathway enzymes. Although a direct correlation between pathogenicity and *O*-linked glycosylation in the AYE strain of *A. baumannii* remains to be elucidated, this work highlights an analogous pathway previously shown to diminish infectivity when disrupted. Future work focusing on inhibiting the *A. baumannii* enzymes responsible for UDP-diNAcBac biosynthesis will strengthen the correlation between pathogenicity and bacterial glycosylation. The rise of this multi-drug resistance strain in the hospital environment is cause for alarm and makes the search for novel virulence targets all that more important. The enzymes responsible for UDP-diNAcBac biosynthesis may well represent novel targets in the struggle against *A. baumannii* resistance.

Acknowledgment

We wish to thank Dr. Angelyn Larkin, Dr. Meredith Hartley, and Austin Travis for critical reading of the manuscript and useful discussions regarding experimental data.

Appendix A. Supplementary data

Supplementary data associated with this article can be found, in the online version, at http://dx.doi.org/10.1016/j.abb.2013.05.011.

References

[1] L. Dijkshoorn, A. Nemec, H. Seifert, Nat. Rev. Microbiol. 5 (2007) 939–951.
[2] F. Perez, A.M. Huher, K.M. Hujer, B.K. Decker, P.N. Rather, R.A. Bonomo, Antimicrob. Agents Chemother. 51 (2007) 3471–3484.
[3] A.Y. Peleg, H. Seifert, D.L. Paterson, Clin. Microbiol. Rev. 21 (2008) 538–582.
[4] D. Vallenet, P. Nordmann, V. Barbe, L. Poirel, S. Mangenot, E. Bataille, C. Dossat, S. Gas, A. Kreimeyer, P. Lenoble, S. Oztas, J. Poulain, B. Sigurens, C. Robert, C. Abergel, J.M. Claverie, D. Raoult, C. Medigue, J. Weissenbach, S. Cruveiller, PLoS One 3 (2008) e1805.
[5] L. Poirel, O. Menuteau, N. Agoli, C. Cattoen, P. Nordmann, J. Clin. Microbiol. 41 (2003) 3542–3547.
[6] P.E. Fournier, D. Vallenet, V. Barbe, S. Audic, H. Ogata, L. Poirel, H. Richet, C. Robert, S. Mangenot, C. Abergel, P. Nordmann, J. Weissenbach, D. Raoult, J.M. Claverie, PLoS Genet. 2 (2006) e7.
[7] M.D. Adams, K. Goglin, N. Molyneaux, K.M. Hujer, H. Lavender, J.J. Jamison, I.J. MacDonald, K.M. Martin, T. Russo, A.A. Campagnari, A.M. Hujer, R.A. Bonomo, S.R. Gill, J. Bacteriol. 190 (2008) 8053–8064.
[8] J. Nothaft, C.M. Szymanski, Nat. Rev. Microbiol. 8 (2010) 765–778.
[9] J. Kelly, H. Jarrell, L. Millar, L. Tessier, L.M. Fiori, P.C. Lau, B. Allan, C.M. Szymanski, J. Bacteriol. 188 (2006) 2427–2434.
[10] A.V. Karlyshev, P. Everest, D. Linton, S. Cawthraw, D.G. Newell, B.W. Wren, Microbiology 150 (2004) 1957–1964.
[11] I.C. Schoenhofen, D.J. McNally, E. Vinogradov, D. Whitfield, N.M. Young, S. Dick, W.W. Wakarchuck, J.R. Brisson, S.M. Logan, J. Biol. Chem. 281 (2006) 723–732.
[12] N.B. Olivier, M.M. Chen, J.R. Behr, B. Imperiali, Biochemistry 45 (2006) 13659–13669.
[13] A. Vik, F.E. Aas, J.H. Anonsen, S. Bilsborough, A. Schneider, W. Egge-Jacobsen, M. Koomey, Proc. Natl. Acad. Sci. U.S.A. 106 (2009) 4447–4452.
[14] M.D. Hartley, M.J. Morrison, F.E. Aas, B. Borud, M. Koomey, B. Imperiali, Biochemistry 50 (2011) 4936–4948.
[15] J.A. Iwashkiw, A. Seper, B.S. Weber, N.E. Scott, E. Vinogradov, C. Stratilo, B. Reiz, S.J. Cordwell, R. Whittal, S. Schild, M.F. Feldman, PLoS Pathog. 8 (2012) e1002758.
[16] A. Larkin, B. Imperiali, Biochemistry 48 (2009) 5446–5455.
[17] M.M. Chen, E. Weerapana, E. Ciepichal, J. Stupak, C.W. Reid, E. Swiezewska, B. Imperiali, Biochemistry 46 (2007) 14342–14348.
[18] A. Krogh, B. Larsson, G. von Heijne, E.L. Sonnhammer, J. Mol. Biol. 305 (2001) 567–580.
[19] K.J. Glover, E. Weerapana, M.M. Chen, B. Imperiali, Biochemistry 45 (2006) 5343–5350.
[20] I.C. Schoenhofen, V.V. Lunin, J.P. Julien, Y. Li, E. Ajamian, A. Matte, M. Cygler, J.R. Brisson, A. Aubry, S.M. Logan, S. Bhatia, W.W. Wakarchuk, N.M. Young, J. Biol. Chem. 281 (2006) 8907–8916.
[21] J. Badger, J.M. Sauder, J.M. Adams, S. Antonysamy, K. Bain, M.G. Bergseid, S.G. Buchanan, M.D. Buchanan, Y. Batiyenko, J.A. Christopher, S. Emtage, A. Eroshkina, I. Feil, E.B. Furlong, K.S. Gajiwala, X. Gao, D. He, J. Hendle, A. Huber, K. Hoda, P. Kearins, C. Kissinger, B. Laubert, H.A. Lewis, J. Lin, K. Loomis, D. Lorimer, G. Louie, M. Maletic, C.D. Marsh, I. Miller, J. Molinari, H.J. Muller-Dieckmann, J.M. Newman, B.W. Noland, B. Pagarigan, F. Park, T.S. Peat, K.W. Post, S. Radojicic, A. Ramos, R. Romero, M.E. Rutter, W.E. Sanderson, K.D. Schwinn, J. Tresser, J. Winhoven, T.A. Wright, L. Wu, J. Xu, T.J. Harris, Proteins 60 (2005) 787–796.
[22] A. Larkin, N.B. Olivier, B. Imperiali, Biochemistry 49 (2010) 7227–7237.
[23] The PyMOL Molecular Graphics System, Version 1.5.0.4 Schrödinger, LLC.
[24] A.M. Waterhouse, J.B. Procter, D.M.A. Martin, M. Clamp, G.J. Barton, Bioinformatics 25 (2009) 1189–1191.
[25] N.B. Olivier, B. Imperiali, J. Biol. Chem. 283 (2008) 27937–27946.
[26] A.H.K. Choi, L. Slamti, F.Y. Avci, G.B. Pier, T. Maira-Litran, J. Bacteriol. 191 (2009) 5953–5963.
[27] F. St Michael, C.M. Szymanski, J. Li, K.H. Chan, N.H. Khieu, S. Larocque, W.W. Wakarchuk, J.R. Brisson, M.A. Monteiro, Eur. J. Biochem. 269 (2002) 5119–5136.
[28] C. Creuzenet, FEBS Lett. 559 (2004) 136–140.
[29] F. Hynne, S. Dano, P.G. Sorensen, Biophys. Chem. 94 (2001) 121–163.
[30] B. Teusink, H. Bachmann, D. Molenaar, Microb. Cell Fact. 10 (Suppl. 1) (2011) S11.
[31] Q. Wang, M.S. Ou, Y. Kim, L.O. Ingram, K.T. Shanmugam, Appl. Environ. Microbiol. 76 (2010) 2107–2114.